Robust RST Controller Design for Induction Motor Drive for Electric Vehicle Application

M. Bendjedia, K. A. Tehrani, Y. Azzouz and H. Shall
Institut de Recherche en Systèmes Electroniques Embarqués (IRSEEM), Ecole Supérieure d'Ingénieurs en Génie Electriques (ESIGELEC) – Technopôle du Madrillet, Saint-Etienne du Rouvray 76800, France.
Moussa.bendjedia@esigelec.fr, kambiz.tehrani@esigelec.fr, yacine.azzouz@esigelec.fr, hanen.shall@esigelec.fr

***Abstract*—This paper presents a new robust control system for induction motor intended for electric vehicle applications (EVA). A new RST controller is designed to accelerate the speed time response without overshoots and to remove the effects of disturbance related to speed sensors. This controller can quickly compensate the load torque disturbance. In order to reduce the measured noise generated by the speed sensor, we proposed an alternative structure based on two control loops. For high-dynamic performance of the control system, we used the indirect stator-flux-oriented control (ISFOC) and the space vector pulse width modulation (SVPWM) techniques. The simulation results show the performance of the proposed solution.**

Keywords— Electric vehicle (EV), induction motor drive; RST controller; internal model; disturbance rejection; indirect stator-flux-oriented control (ISFOC); space vector pulse width modulation (SVPWM).

NOMENCLATURE

v_{ds}, v_{qs}	*d*- and *q*- axis stator voltages.
i_{ds}, i_{qs}	*d*- and *q*- axis stator currents.
Φ_{ds}, Φ_{qs}	*d*- and *q*- axis stator *flux*.
Φ_s	Stator rated flux.
R_s, R_r	Stator and rotor winding resistances.
L_s, L_r, M	Stator, rotor and mutual inductances.
J, f	Rotor inertia and viscous friction coefficient.
N_p	Number of the pole pairs.
ω_s, ω_r, ω_{sl}	Synchronous, rotor and slip angular speed.
Ω, Ω_m	Real and measured mechanical rotor speed.
T_e, T_L	Electromagnetic and load torque.
V_{DC}	Inverter input DC voltage.
τ_s , τ_r	Stator and rotor time constant.
p	Laplace operator.
*	Reference quantities.
T	Sampling period.
ω_0	Natural frequency.
ζ	Damping coefficient.
k	Constant.
$p(t)$	Speed sensor noise.

I. INTRODUCTION

To reduce greenhouse gas emissions generated by cars, many industrials are encouraged to develop electric or hybrid vehicles [1]. One of the disadvantages of the EV is the energy storage because the batteries have a limited range, and take a long time to charge [2].

This work is part of a research project concerning the development of a new extended range of urban EV based multi-source system. The speed of this new electrical vehicle is limited to 50km/h. The main goal for this EV is to increase the energy autonomy. To meet this need, we added two source of energy to recharge the batteries. The first source is an alternator connected to an internal combustion engine and the second source is solar panels.

On the other hand, the EV drive systems require fast torque response and wide speed range with high efficiency. The vehicle behavior must be tested on different speed-torque conditions according to European Driving Cycles (highway, rural road, traffic and urban) [3], [4].

The major types of electric motor used for EVs traction are DC motor, induction motor, permanent magnet synchronous motor and switched reluctance motor [5]. Cage induction motors are widely accepted as the most potential candidate for EVA thanks to their reliability, ruggedness, low maintenance and low cost, [6]. In [7], a methodology for presizing the induction motor propulsion of an EV is proposed in order to find the minimum weight, volume, and cost that meet the design constraints with minimum power under driving cycles.

The most significant control methods for an induction motor are scalar control (V/f=Volts/Hertz), direct torque control (DTC) and indirect field oriented control (IFOC). In the scalar control technique, the voltage is required to be proportional to frequency so that the stator flux remains constant. Scalar control method is widely used in industry because of its simplicity. This open loop control produces good steady state performance but poor dynamic response. The DTC does not require any; coordinate transformation, current regulator and PWM signals generators. In spite of its simplicity, DTC allows a good torque control in steady-state and transient state. However, the DTC presents some disadvantages such as high current and torque ripples, variable switching frequency and high noise level at low speed [8]. The IFOC is the best control technique to control an induction motor for EVA [9]. The dynamic response of the induction motor can be improved using the SVPWM technique which reduces the current and voltage harmonics.

978-1-4799-3602-1/14/$31.00 ©2014 IEEE

A PID controller is less robust than a RST controller against disturbances. The RST controller [10], [11] is an efficient strategy of digital control and it has been used in many applications. For HEV, it has been applied to the DC/DC converter to ensure energy management between supercapacitor and battery [12]. In [13], the RST controller is designed to control the PWM rectifier for battery charger of the EV. The RST controller is also used in renewable energy such as wind turbine [14] and photovoltaic [15]. In [16], this controller has been proposed to control the rotor position of the hybrid step motor where a high accuracy of positioning is required.

For high-dynamic performance, field oriented control (FOC) is used for induction motor drive. This technique requires speed and currents sensors. The growing of electrical systems embedded in the vehicle imposes to pay more attention and thorough study of the electromagnetic compatibility. Both radiated and conducted electromagnetic interference can affect the measured quantities. However, it is necessary to design a robust controller that can reject the maximum of these disturbances or to decrease the impacts of disturbance.

In this paper, we propose a robust control system for an induction motor used in electric vehicle (EV). We designed an advanced RST controller for speed control and we used the ISFOC and the SVPWM techniques in order to obtain high-dynamic performance. To ensure correct operation of speed control despite the disturbances of the speed sensors, we design an RST controller with two controls loops.

The output of the speed loop is the current reference and a simple PI controller is used for the current loop.

II. STATOR FLUX ORIENTATION CONTROL

A. Stator flux orientation model

The dynamic model of the induction machine expressed in the *d-q* axis reference frame is given as follows [17].

$$\begin{cases} \dfrac{d\Phi_{ds}}{dt} = \omega_s \Phi_{qs} - R_s i_{ds} + v_{ds} \\ \dfrac{d\Phi_{qs}}{dt} = -\omega_s \Phi_{ds} - R_s i_{qs} + v_{qs} \\ \dfrac{di_{ds}}{dt} = \dfrac{1}{\sigma\tau_r L_s}\Phi_{ds} + \dfrac{\omega_r}{\sigma L_s}\Phi_{qs} - \dfrac{(\tau_s+\tau_r)1}{\sigma\tau_s\tau_r} i_{ds} + \omega_{sl} i_{qs} + \dfrac{1}{\sigma L_s} v_{ds} \\ \dfrac{di_{qs}}{dt} = -\dfrac{\omega_r}{\sigma L_s}\Phi_{ds} + \dfrac{1}{\sigma\tau_r L_s}\Phi_{qs} - \omega_{sl} i_{ds} - \dfrac{(\tau_s+\tau_r)1}{\sigma\tau_s\tau_r} i_{qs} + \dfrac{1}{\sigma L_s} v_{qs} \\ \dfrac{d\omega_r}{dt} = \dfrac{N_p^2}{J} i_{qs}\Phi_{ds} - \dfrac{N_p^2}{J} i_{ds}\Phi_{qs} - \dfrac{f}{J}\omega_r - \dfrac{N_p}{J} T_L \end{cases} \quad (1)$$

where $\omega_{sl} = \omega_s - \omega_r$, $\tau_r = \dfrac{L_r}{R_r}$, $\tau_s = \dfrac{L_s}{R_s}$ and $\sigma = 1 - \dfrac{M^2}{L_s L_r}$

The ISFOC allows separating the closed loop decoupling control of both flux and torque. The *d*-axis is chosen on the flux axis, so all the flux is aligned along this axis, therefore we can write:

$$\Phi_{ds} = \Phi_s ; \quad \Phi_{qs} = 0 \quad (2)$$

The torque is controlled by using the *q*-axis current

$$T_e = N_p \Phi_{ds} i_{qs} \quad (3)$$

By using (1) and (2), the *d* and *q*-axis command stator currents can be expressed as

$$\begin{aligned} i_{ds}^* &= \frac{(1+\tau_r p)\phi_s^* + L_s\sigma\tau_r\omega_{sl}^* i_{qs}^*}{L_s(1+\sigma\tau_r p)} \\ i_{qs}^* &= \frac{\tau_r\omega_{sl}^*(\phi_s^* - L_s\sigma i_{ds}^*)}{L_s(1+\sigma\tau_r p)} \end{aligned} \quad (4)$$

The *d* and *q*-axis command stator voltage are given by

$$\begin{aligned} v_{ds} &= \sigma L_s\left(p + \frac{\tau_s+\tau_r}{\sigma\tau_s\tau_r}\right) i_{ds}^* - \frac{1}{\tau_r}\phi_s^* - \sigma L_s\omega_{sl}^* i_{qs}^* \\ v_{qs} &= \sigma L_s\left(p + \frac{\tau_s+\tau_r}{\sigma\tau_s\tau_r}\right) i_{qs}^* + \frac{\omega_r}{\tau_r}\phi_s^* + \sigma L_s\omega_{sl}^* i_{ds}^* \end{aligned} \quad (5)$$

B. Drive control structure

The proposed control of the induction motor is presented in Fig. 1. From (5), we can see that stator voltage components are coupled by the *d*- and *q*- back electromotive force (EMF) given by

$$\begin{aligned} v_d^{dec} &= -\frac{1}{\tau_r}\phi_s^* - \sigma L_s\omega_{sl}^* i_{qs}^* \\ v_d^{dec} &= \frac{\omega_r}{\tau_r}\phi_s^* + \sigma L_s\omega_{sl}^* i_{ds}^* \end{aligned} \quad (6)$$

The *d*-axis voltage depends on *q*-axis current, and *q*-axis voltage depends also on *d*-axis current. In order to have linear terms, we applied the feedforward decoupling method [18]. Therefore, the $d-q$ axis stator voltages (5) become

$$\begin{aligned} v_d &= v_{ds} - v_{ds}^{dec} = \sigma L_s\left(p + \frac{\tau_s+\tau_r}{\sigma\tau_s\tau_r}\right) i_{ds}^* \\ v_q &= v_{ds} - v_{qs}^{dec} = \sigma L_s\left(p + \frac{\tau_s+\tau_r}{\sigma\tau_s\tau_r}\right) i_{qs}^* \end{aligned} \quad (7)$$

The SVPWM is more sophisticated technique to provide a higher voltage to the induction motor compared with a classical PWM. The basis of SVPWM is different from that of sine pulse width modulation (SPWM). SPWM aims to achieve symmetrical 3-phase sine voltage waveforms of adjustable voltage and frequency, while the SVPWM uses the eight fundamental voltage vectors to realize variable frequency of voltage and speed adjustment and it offers better DC bus utilization [19].

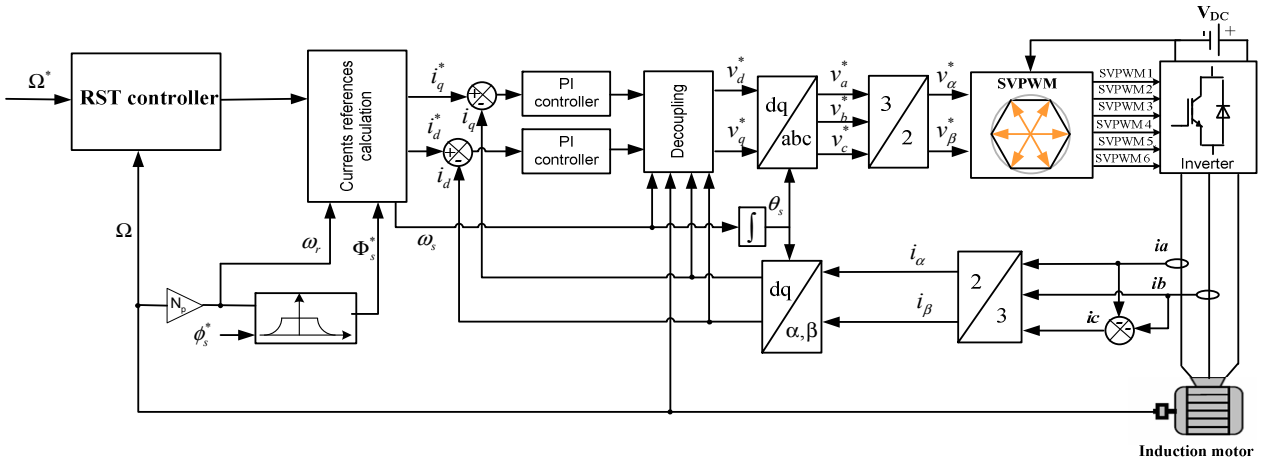

Fig. 1. Block diagram of the proposed control of induction motor

III. RST CONTROLLER

The RST controller [10], [11] consists in three numerical polynomials in discrete time domain noted *S(z)*, *R(z)* and *T(z)* as shown in Fig. 2. The synthesis of this controller consists to find the parameters of these polynomials in order to achieve the desired performances of the closed loop system. The controller is proposed for speed control loop (current reference computation), therefore the discrete mechanic model is needed.

A. Discrete mechanical model

By considering only the mechanical part, i.e the last equation of (1) taking into account (3), the motor model in the continuous domain is given by

$$F(p)=\frac{\Omega(p)}{i_{qs}^{*}(p)}=\frac{K}{p+p_1} \tag{8}$$

where $\omega_r = N_p\Omega$; $K=\dfrac{N_p\Phi_s}{J}$ and $p_1=\dfrac{f}{J}$

The load torque T_L is considered just as disturbance and we will examine its influence later.

By using a ZOH (Zero order hold), the discrete model of (8) is given by

$$H(z)=Z\left[B_0(p)F(p)\right]=\left(1-z^{-1}\right)Z\left[\frac{F(p)}{p}\right] \tag{9}$$

After development of (9), we obtain

$$H(z)==\frac{B(z)}{A(z)}=\frac{K_1\left(1-z_1\right)z^{-1}}{1-z_1z^{-1}}=\frac{b_0+b_1z^{-1}}{a_0+a_1z^{-1}} \tag{10}$$

where

$$K_1=\frac{K}{p_1},\ z_1=e^{-p_1T},\ b_0=0,\ b_1=K_1\left(1-z_1\right),\ a_0=1,\ a_1=-z_1$$

B. RST controller design

The RST controller consists of the functional block diagram (FBD), as shown in Fig. 2. The output speed can be expressed as follows:

$$\Omega=\frac{TB}{AS+BR}\Omega^{*}-\frac{AS}{AS+BR}T_L+\frac{BR}{AS+BR}b \tag{11}$$

For simplification the variable z is not presented in (11). First we assume that the measured noise *b(z)* is null.

The design of RST controller consists to find the parameters of the polynomials *R(z), S(z)* and *T(z)* in order to achieve the desired performances, in terms of tracking accuracy and disturbance rejection. *S(z)* and *R(z)* appear in the denominator of (11), therefore we can obtain their parameters by solving the Bezout equation defined by:

$$P(z)=A(z)S(z)+B(z)R(z) \tag{12}$$

P(z) is the characteristic polynomial (i.e., the poles in closed loop system). The choice of the degrees of the polynomials is an important step in the design of the RST controller. It is a compromise between performance and complex controller. We choose a strictly proper controller [11] in order to achieve a good accuracy adjustment. So the degrees of the polynomials *P(z)*, *R(z)* and *S(z)* are given by

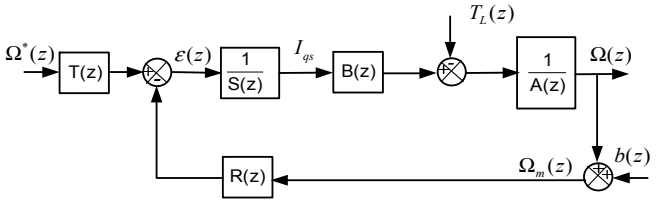

Fig. 2. Block diagram of RST controller

$$d^{\circ}(P) = 2d^{\circ}(A) + 1 = 3$$
$$d^{\circ}(S) = d^{\circ}(A) + 1 = 2 \quad (13)$$
$$d^{\circ}(R) = d^{\circ}(A) = 1$$

Thus, the polynomials *P(z)*, *R(z)* and *S(z)* can be written as:

$$P(z) = 1 + p_1 z^{-1} + p_2 z^{-2} + p_3 z^{-3} \quad (14)$$
$$S(z) = (1 - z^{-1})(s_0 + s_1 z^{-1}) \quad (15)$$
$$R(z) = r_0 + r_1 z^{-1} \quad (16)$$

An integration action is introduced in *S(z)* in order to ensure a load torque disturbance rejection.

The choice of the roots of the polynomial *P(z)* is done according to the desired performances for the closed loop system. The coefficients of *S(z)* et *R(z)* are obtained by imposing three poles in a closed-loop system . We choose a pair of complex conjugate poles that the imaginary part is equal to the negative real part and the third pole also is equal to the negative real part. In this case, the overshoot created by the pair of the complex conjugate poles is compensated by the real pole. The transfer function of the second order system in the continuous domain is defined by:

$$H_c(p) = \frac{\omega_0^2}{p^2 + 2\zeta\omega_0 p + \omega_0^2} \quad (17)$$

If $\zeta < 1$, the poles of $H_c(p)$ are given by:

$$p_{1,2} = -\zeta\omega_0 \pm j\omega_0\sqrt{1-\zeta^2} \quad (18)$$

To get the real part equal to the imaginary part, it is necessary to take $\zeta = 0.707$. Thus, the selected poles in the continuous domain for polynomial *P(z)* in equation (14) are:

$$p_{1,2} = -\zeta\omega_0 \pm j\zeta\omega_0 \text{ and } p_3 = -\zeta\omega_0 \quad (19)$$

The polynomial *P(z)* that contains the poles can be written as:

$$P(z) = (1 + a_{d1}z^{-1} + a_{d2}z^{-2})(1 + z_3 z^{-1}) \quad (20)$$

where $a_{d1} = -2e^{-\zeta\omega_0 T}\cos(\omega_a T)$; $a_{d1} = e^{-2\zeta\omega_0 T}$; $z_3 = -e^{-\zeta\omega_0 T}$

The Bezout equation (12) becomes:

$$P(z) = (a_0 + a_1 z^{-1})(1 - z^{-1})(s_0 + s_1 z^{-1}) + (b_0 + b_1 z^{-1})(r_0 + r_1 z^{-1}) \quad (21)$$

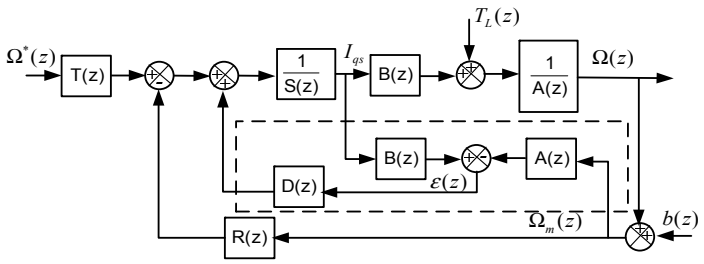

Fig. 3. Block diagram of the modified RST controller.

The identification between (20) and (21) makes it possible to find the coefficients of the two polynomials *R(z)* and *S(z)*.

T(z) can be a constant that guarantee null steady-state error. By using (11) and considering that *S(z)* is null in steady state, *T(z)* can be obtained as follows:

$$T(z) = t_0 = r_0 + r_1 \quad (22)$$

The above designed RST controller can reject the load torque disturbance because we introduced an integration action in the polynomial *S(z)*.

The speed or position sensors are sensitive to temperature and EMI. The sources of EMI in EV can be difficult to find and remedy. EMI radiated noise and conducted cable noise can come from any number of possible sources like the speed drives, power leads and electric motors or command part. The incremental encoder is the most common sensor used in industry application. This kind of sensor provide 5V DC signals, therefore it is sensitive to EMI noises in particular common mode noises. In addition, an EV can interfere with another when they are side by side. However, the speed or position sensors are neither precise or reliable and therefore they can introduce measurement errors and instability of the closed loop control system.

To overcome these problems, sensorless control methods such as nonlinear observer [19] and Kalman filter [20] are widely used in the literature. In these techniques, the mechanical sensor is replaced by a software algorithm that can estimate the rotor speed or position by only measuring the motor currents and voltages.

Moreover, robust controllers can be used for EMI noise mitigation. A good controller should have a fast speed time response, small overshoot, good disturbance rejection and very good stability. The different optimization methods for controllers have been proposed as [21], [22], the design of PID controller with convex-concave optimization [23] and RST controller with convex optimization method [24]. The convex optimization technique allows to find the best controller parameters that can fulfill the desired performance of the closed loop system and to solve the problem of disturbance sensitivity in the closed loop systems.

In this work, we propose an alternative structure based on two control loops as schown in Fig. 3. This structure uses the internal model principle (IMP) which means the inclusion of disturbance model into the controlling structure. The internal

control loop in Fig. 3 (encircled by dotted lines) uses the motor model (10) in order to estimate and compensate the effect of the load torque disturbance (signal *ε(z)*) on the controller variable Ω(z).

By using the motor mechanical model, i.e the last equation of (1) taking into account (3), the load torque disturbance can be estimated as follows:

$$\hat{T}_L = B(z)I_{qs} - A(z)\Omega_m \tag{23}$$

With $\Omega_m = \Omega + b(t)$

$b(t)$ is the measured noise.

The predictive polynomial *D(z)* can be chosen according to the class of load torque disturbances (constant, ramp, parabolic and sinusoidal). The most frequently prediction polynomial is $D(z) = 2 - z^{-1}$ which can reject ramp disturbances; but, it enables also the extraction of slow varying disturbances and even suppression of the effects of low frequency stochastic disturbances [25]. This prediction polynomial can also reject the influence of load torque disturbance on the steady state value of the rotor speed. Note that the use of a digital low-pass filter causes an error in the load torque disturbance estimation and rejection.

The main control loop (speed controller) is designed independently of the internal loop. The coefficients of polynomials *S(z), R(z)* and T(z) are obtained by using the same above procedure (11) - (22) with the same imposed poles (19). However, it is not necessary to introduce an integral action in the polynomial *S(z)* because the load torque disturbance is estimated and rejected by the inner loop. In order to have a null steady state error with reduction of the measured noise *b(t)*, we propose the following polynomials.

$$S(z) = s_0 + s_1 z^{-1} + s_3 z^{-2} \tag{23}$$

$$R(z) = r_0 \left(1 - z^{-1}\right) \tag{24}$$

The polynomial *T(z)* can be expressed as

$$T(z) = \frac{P(1)}{B(1)} \tag{25}$$

For this system, the robustness is achieved by the operation of the inner loop which suppress as much as possible the effects of generalized disturbance (external disturbance and uncertainty of the nominal model (10) on the rotor speed. The advantage of the structure of Fig. 3 versus classical RST controller is the estimation of the load torque disturbance taking into account the reduction of the measurement noise.

IV. SIMULATION RESULTS

This section presents the simulation results obtained from speed control of the induction motor drives as shown in Fig. 1. The simulation is realized on Matlab/Simulink platform. The RST controller (section III) is designed in the discrete time (z-domain). Therefore, the system shown in Fig. 1 is transformed in this domain. The induction motor parameters are given in table I of appendix. The total sampling time is 62.5 µs. The stator field oriented control technique is realized with an SVPWM carrier frequency of 16 kHz. For comparison with the RST controller, we used an integral-proportional (IP) controller [18]. The choice of the parameters of currents controllers is done according to the desired performances for the closed loop system by imposing the natural frequency and the damping ratio.

Firstly, we present the simulation results without speed perturbation (Fig. 4 and 5). Fig. 4 shows the comparison between the proposed RST controller and the IP controller. The reference rotor speed is set at the nominal speed 1430 rpm with a step load torque T_L = 10 Nm applied to the system at time t = 1s and removed at time t = 2s. At time t = 3 s, the reference speed is changed from 1430 rpm to -500 rpm and the load torque is applied again at time t = 4s. It can be seen that both controllers give good results, in term of overshoot. Note that RST controller is faster for tracking and load torque disturbance rejection. This is due to the design of RST controller with the selected three poles (19) in order to accelerate the speed time response without overshoot.

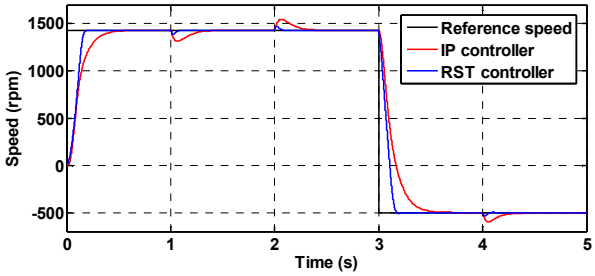

Fig. 4. Speed response time with RST and IP controllers.

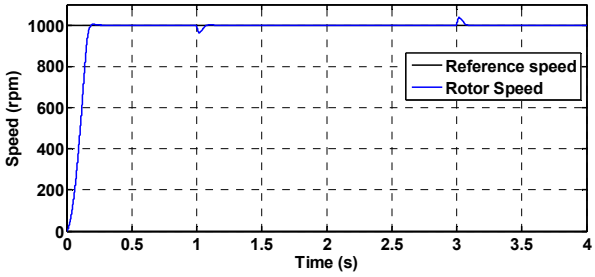

a) Speed response time

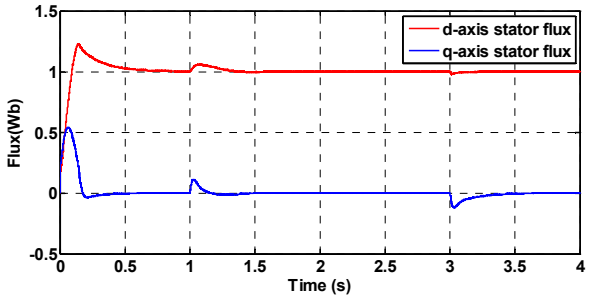

b) *d*- and *q*- axis stator flux (Φ_{ds}, Φ_{qs})

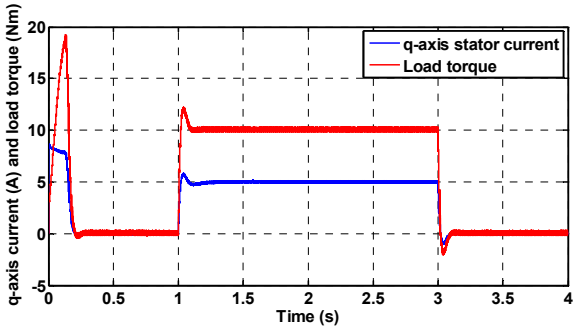

c) *q*- axis stator current and load torque (i_{qs}, T_L)

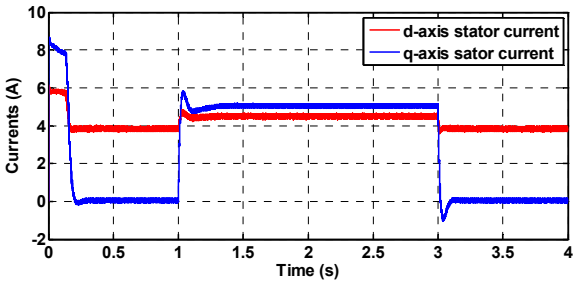

d) *d*- and *q*- axis stator currents (i_{ds}, i_{qs})

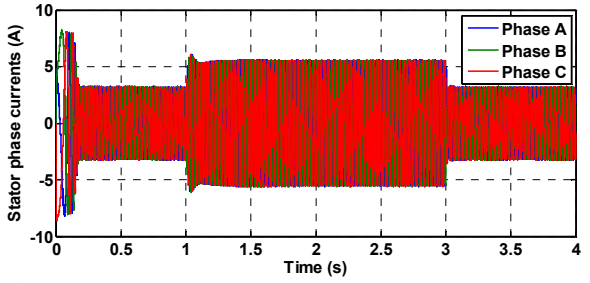

e) Phase currents (i_a, i_b, i_c)

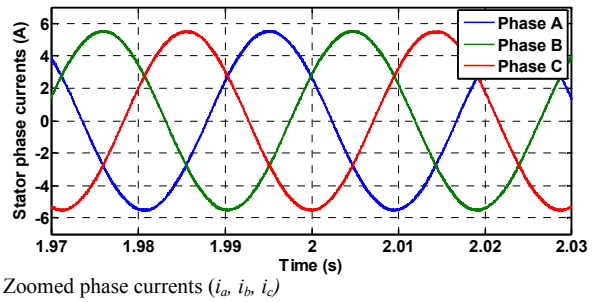

f) Zoomed phase currents (i_a, i_b, i_c)

Fig. 5. Simulation results of RST controller with speed reference of 1000 rpm and load torque applied at t = 1s and removed at t = 3s.

Fig. 5 presents the simulation results with a speed reference of 1000 rpm with the RST controller. In this case, the load torque T_L = 10 Nm is applied at t = 1 s and removed at t = 3 s. Fig. 5 (b) shows that Φ_{ds} is set to its reference which is the total flux ($\Phi_s^* = 1$) but Φ_{qs} is maintained at zero as presented in (2). In Fig. 5 (c), we can see that the motor torque is proportional to the *q*-axis stator current i_{qs} as given in (3). Fig. 5 (d) and (e) show, the stator currents in the *d*-*q* axis (i_{ds}, i_{qs}) and in the fixed reference frame (i_a, i_b, i_c) respectively. The simulation results show that the RST controller and the ISFOC exhibit good performances for induction motor drive.

Fig. 6 shows the simulation results of the induction motor control based on the modified RST controller (Fig. 3). The reference speed is set at 1430 rpm with a step load torque T_L = 10Nm applied at time t = 1s and removed at t = 3s. The comparison between Fig. 5 (a) and Fig. 6 (a) shows the performances of the two controllers structure (RST and modified RST), in terms of tracking, and load torque disturbance rejection.

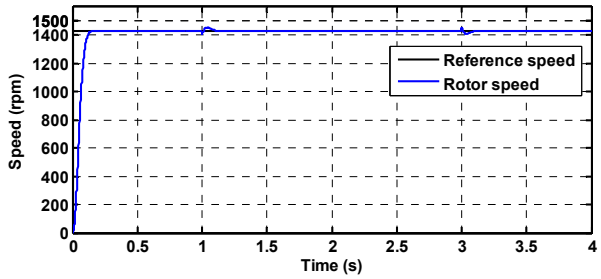

a) Speed time response

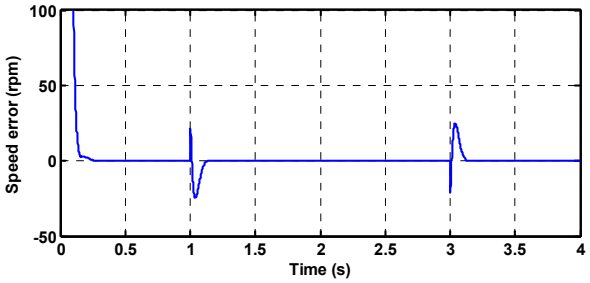

b) Speed error (Ω^*-Ω)

Fig. 6. Simulation results of the modified RST controller.

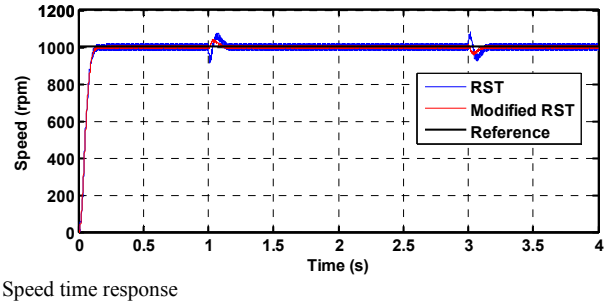

a) Speed time response

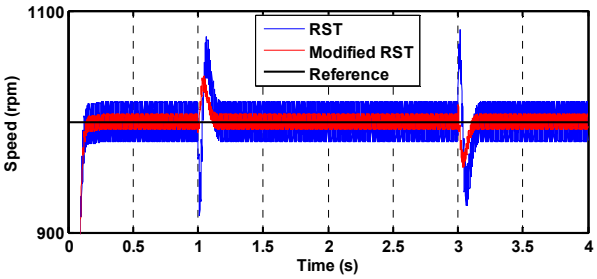

b) Zoomed speed time response.

Fig. 7. Comparision of RST and modified RST controllers in presence of measure noise.

Fig. 7 shows the speed time response of the two controllers, with a sinusoidal perturbation added to the speed sensor. It can be seen that the modified RST controller is well suitable for noise measurement reduction.

V. CONCLUSION

In this paper a robust control system for induction motor drive for EV application is proposed. An advanced RST controller is designed for speed control system. This controller can accelerate the response time without overshoot thanks to proper poles placement of the closed loop system. Due to the lack of reliability of speed sensor, we proposed a modified RST controller that can estimate and reject the load torque disturbance taking into account the reduction of speed measurement noise. This modified RST controller is based on the internal model control design (IMCD) with two loops. For high-dynamic performance of the control system, we used the ISFOC and the SVPWM techniques. Simulation results show the advantage of the RST controller in comparison to IP controller, in terms of tracking and load torque disturbance rejection. The simulation results show the excellent control of induction motor drive used in electric vehicle application.

APPENDIX

TABLE I. INDUCTION MOTOR PARAMETERS

Specifications		***Parameters***	
Rated power	3kW	R_s	2.3 Ω
Rated voltage	380V	R_r	1.55 Ω
Rated current	6.6A	L_s	0.261 H
Rated frequency	50Hz	L_r	0.261 H
Number of pole pairs	2	M	0.249 H
Rated speed	1430 r/min	J	0.02 kg/m^2
		f	0.0007 Nm.s./rad

ACKNOWLEDGMENT

The authors would like to thank the region « Haute-Normandie » and the « Fonds Européen de Développement Régional (FEDER) » for the financial support under VIRTUOSE project.

REFERENCES

[1] C. C. Chan, "The state of the art of electric and hybrid vehicles," in *proc. IEEE Conf.*, vol. 90, no. 2, pp. 247– 275, Feb. 2002.

[2] H. B. Jensen, E. Schaltz, P. S. Koustrup, S. J Andreasen, S. K. Kaer, "Evaluation of fuel-cell range extender impact on hybrid electrical vehicle performance," *IEEE Trans. Veh. Technol.*, vol. 62, no. 1, pp. 50–60, Jan. 2013.

[3] M. Andre, R. Joumard, R. Vidon, P. Tassel, P. Perret, " Real-world european driving cycles, for measuring pollutant emissions from high and low-powered cars," in *proc. ETTAP09 Conf.,* pp. 5944–5953, Oct. 2009.

[4] A. Berthon, F. Gustin, M. Bendjedia, J. M. Morelle, G. Coquery, "Inverter components reliability tests for hybrid electrical vehicles," in *Proc. IPEMC'09 Conf.,* pp. 763-768, 17–20 May 2009.

[5] J. G. W. West, "DC, induction, reluctance and PM motors for electric vehicles," *IEE Power Engineering Journal*, vol. 8, no. 2, pp. 77–88, Apr. 1994.

[6] M. Zeraoulia, M. E. H. Benbouzid and D. Diallo, "Electric motor drive selection issues for HEV propulsion systems: a comparative study," *IEEE Trans. Veh. Technol.*, vol. 55, no 6, pp. 1756 –1764, Nov. 2006.

[7] B. Tabbache, A. Kheloui, M. E. H. Benbouzid, D. Diallo, "Design and control of the induction motor propulsion of an electric vehicle," in *proc. IEEE/VPPC Conf.,* Sep. 2010, pp. 1–6.

[8] D. Casadei, F. Profumo, G. Serra, A. Tani, "FOC and DTC: two viable schemes for induction motors torque control," *IEEE Trans. Power. Electron.*, vol. 17, no. 5, pp. 779–787, Sep. 2002.

[9] O. Ellabban, J. Van Mierlo, P. Lataire, "A comparative study of different control techniques for an induction motor fed by a Z-source inverter for electric vehicles," in *proc. POWERENG'11 Conf.,* May 2011, pp. 1–7.

[10] J. D. Landau, Commande des systèmes : conception, identification et mise en oeuvre, Paris, Hermès, 2002.

[11] R. Longchamp, Commande numérique des systèmes dynamiques, Presses Polytechniques et Universitaire Romandes, 2006.

[12] M. B. Camara, H. Gualous, F. Gustin, A. Berthon, B. Dakyo. "DC/DC converter design for supercapacitor and battery power management in hybrid vehicle applications - polynomial control strategy", *IEEE Trans. Ind. Electron*, Vol. 57, no. 2, pp. 587–597, Feb. 2010.

[13] S. Lacroix, M. Hilairet, E. Laboure, "Design of a battery-charger controller for electric vehicle based on RST controller," in *proc. VPPC'11 Conf.*, pp. 1-6, 6–9 Sept. 2011.

[14] A. Pintea, D. Popescu, P. Borne, "Robust control for wind power systems," in *proc. MED'10 Conf.*, pp. 1085–1091, 23–25 June 2010.

[15] P. Vongkoon, P. Liutanakul, "Digital R-S-T controller for current loop control of DC/DC buck converter: a photovoltaic (PV) array simulator under partial shading condition," in *proc. ECTI-CON'12 Conf.*, pp. 1–4, 16–18 May 2012.

[16] M. Bendjedia, Y. Aït-Amirat, B. Walther and A. Berthon, "Digital step motor drive with EKF estimation of speed and rotor position," *International Review of Electrical Engineering (IREE)*, vol. 2, no 3, pp. 455–465, May–June 2007.

[17] Y. Agrebi, M. Triki,Y. Koubaa et M. Boussak, "Rotor speed estimation for indirect stator flux oriented induction motor drive based on MRAS scheme," *Journal of Electrical Systems (JES)*, vol. 3, no 3 pp. 131–143, 2007.

[18] M. Boussak, K. Jarray, "A high-performance sensorless indirect stator flux orientation control of induction motor drive," *IEEE Trans. Ind. Electron.*, vol. 53, no. 1, pp. 41–49, Feb. 2006.

[19] A. Khlaief, M. Bendjedia, M. Boussak, M. Gossa, "A nonlinear observer for high performance sensorless speed control of IPMSM drive," *IEEE Trans. Power Electron.*, vol. 27, no. 6, pp. 3028–3040, Jun. 2012.

[20] M. Bendjedia, Y. Ait-Amirat, B. Walther, A. Berthon, "Position control of a sensorless stepper motor," *IEEE Trans. Power Electron.*, vol. 27, no. 2, pp. 578–587, Feb. 2012.

[21] S. Boyd and L. Vandenberghe, Convex optimization, Cambridge University Press, 2004.

[22] J. Langer, and I. D. Landau, "Combined pole placement/sensitivity function shaping method using convex optimization criteria," *Automatica journal*, vol. 35, no. 6, pp. 1111–1120, Jan. 2003.

[23] M. Hast, K. J. Astrom, B. Bernhardsson, S. Boyd, "PID design by convex-concave optimization," in *proc. ECC'13 Conf.,* Jul. 2013, pp. 4460–4465.

[24] M. S. Matijević, R. Sredojević, V. M. Stojanović, "Robust RST controller design by convex optimization'', *Electronics*, vol. 15, no. 1, pp. 24–29, 2011.

[25] M. S. Matijević, R. Stojić, M. Stefanović, "Application of internal models in the design of digitally controlled electrical drives'', *Electronics*, vol. 6, no. 2, pp. 31–36, 2002.